Crystal structure determination and dynamic studies of Mycobacterium tuberculosis Cytidine deaminase in complex with products

ARTICLE *in* ARCHIVES OF BIOCHEMISTRY AND BIOPHYSICS · FEBRUARY 2011

Impact Factor: 3.02 · DOI: 10.1016/j.abb.2011.01.022 · Source: PubMed

Archives of Biochemistry and Biophysics 509 (2011) 108–115

Contents lists available at ScienceDirect

Archives of Biochemistry and Biophysics

journal homepage: www.elsevier.com/locate/yabbi

Crystal structure determination and dynamic studies of *Mycobacterium tuberculosis* Cytidine deaminase in complex with products

Zilpa A. Sánchez-Quitian [a,b], Luís F.S.M. Timmers [b,c], Rafael A. Caceres [c,d], Jacqueline G. Rehm [a], Claudia E. Thompson [c], Luiz A. Basso [a], Walter F. de Azevedo Jr. [b,c,*], Diógenes S. Santos [a,*]

[a] Centro de Pesquisas em Biologia Molecular e Funcional (CPBMF), Instituto Nacional de Ciência e Tecnologia em Tuberculose (INCT-TB), Pontifícia Universidade Católica do Rio Grande do Sul (PUCRS), Av. Ipiranga 6681, Porto Alegre, RS 90619-900, Brazil
[b] Programa de Pós Graduação em Biologia Celular e Molecular, Pontifícia Universidade Católica do Rio Grande do Sul, Porto Alegre, RS, Brazil
[c] Facultade de Biociencias, Instituto Nacional de Ciência e Tecnologia em Tuberculose (INCT-TB), Laboratorio de Bioquimica Estrutural (LaBioQuest), Pontifícia Universidade Católica do Rio Grande do Sul (PUCRS), Av. Ipiranga 6681, Porto Alegre, RS 90619-900, Brazil
[d] Programa de Pós Graduação em Medicina e Ciências da Saúde, Pontifícia Universidade Católica do Rio Grande do Sul, Porto Alegre, RS, Brazil

ARTICLE INFO

Article history:
Received 28 December 2010
and in revised form 27 January 2011
Available online 2 February 2011

Keywords:
Tuberculosis
Cytidine deaminase
Crystallography
Molecular dynamics

ABSTRACT

Cytidine deaminase (CDA) is a key enzyme in the pyrimidine salvage pathway. It is involved in the hydrolytic deamination of cytidine or 2′-deoxycytidine to uridine or 2′-deoxyuridine, respectively. Here we report the crystal structures of *Mycobacterium tuberculosis* CDA (MtCDA) in complex with uridine (2.4 Å resolution) and deoxyuridine (1.9 Å resolution). Molecular dynamics (MD) simulation was performed to analyze the physically relevant motions involved in the protein–ligand recognition process, showing that structural flexibility of some protein regions are important to product binding. In addition, MD simulations allowed the analysis of the stability of tetrameric MtCDA structure. These findings open-up the possibility to use MtCDA as a target in future studies aiming to the rational design of new inhibitor of MtCDA-catalyzed chemical reaction with potential anti-proliferative activity on cell growth of *M. tuberculosis*, the major causative agent of tuberculosis.

Introduction

Cytidine deaminase (CDA[1], EC 3.5.4.5, systematic name: cytidine aminohydrolase), which is also known as cytidine nucleoside deaminase, catalyzes the hydrolytic deamination of cytidine or 2′-deoxycytidine to, respectively, uridine or 2′-deoxyuridine (Fig. 1) [1,2]. The *cdd*-encoded CDA plays an important role in the pyrimidine salvage pathway. The latter serves two different functions: (1) scavenge pyrimidine compounds for nucleotide synthesis, and (2) degradation of pyrimidine compounds leading to generation of compounds that serve as carbon and nitrogen sources [3]. In addition, CDA is found in the metabolism of a number of analogues of cytosine nucleoside used as antitumoral and antiviral agents, leading to their pharmacological inactivation [3].

Biochemical and structural studies of CDAs from different organisms have led to the understanding of the enzyme reaction mechanism. CDA contains an active site zinc ion that is essential for catalysis, which is coordinated to a nucleophilic water/hydroxide [4]. Different oligomeric states were observed among CDAs from diverse species. Two groups can be identified, the homodimeric CDAs, such as in *Escherichia coli* [5], and the homotetrameric CDAs, such as in *Saccharomyces cerevisiae* [6], human [2] *Bacillus subtillis* [7] and *Mycobacterium tuberculosis* [8].

The three-dimensional structure of *M. tuberculosis* CDA has been previously solved at 2.0 Å resolution and shown to be composed of four identical subunits, each monomer comprising a single domain with five β-strands and five α-helices [8]. Secondary structural elements are arranged in a three-layer core α–β–α domain with mixed β-sheet of five strands, the last two strands of this structure form a β-wing flexible region.

Sequence alignment of CDAs from different organisms has shown relationships among residues that mediate substrate binding and are conserved in all sequences, in agreement with results obtained from crystal structure determination. For instance MtCDA contained one zinc atom per subunit coordinated by three cysteines (Cys56, Cys89, and Cys92), one glutamate (Glu58) and a water molecule [8]. The same pattern was observed in *B. subtillis* CDA [9].

As the first step toward structural and functional MtCDA characterization, we have previously determined the crystal structure of tetrameric *M. tuberculosis* CDA in the absence of substrate/product ligands [8]. Here we describe two refined crystal structures of

* Corresponding authors. Address: Av. Ipiranga 6681, TecnoPUC, Prédio 92A, Porto Alegre, RS 90619-900, Brazil. Fax: +55 51 33203629.
E-mail addresses: walter@azevedolab.net, wfdaj@uol.com.br (W.F. de Azevedo Jr), diogenes@pucrs.br (D.S. Santos).

[1] *Abbreviations used:* CDA, cytidine deaminase; URD, uridine; dURD, deoxyuridine; dCYT, deoxycytidine; PCA, principal component analysis; TB, tuberculosis; MTB, *Mycobacterium tuberculosis*.

0003-9861/$ - see front matter © 2011 Elsevier Inc. All rights reserved.
doi:10.1016/j.abb.2011.01.022

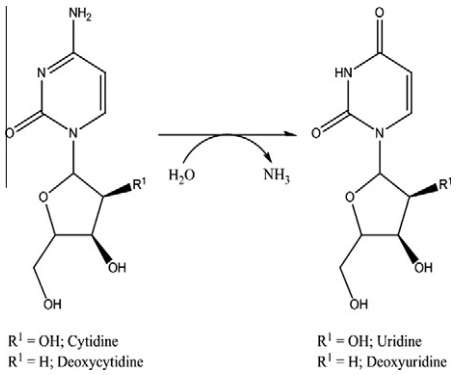

Fig. 1. Chemical reaction catalyzed by MtCDA.

MtCDA in complex with products. These data provide new structural information on the mechanism of active site closure upon ligand binding, and highlight the residues essential for catalysis. Furthermore, molecular dynamics (MD) simulation was performed to analyze the physically relevant molecular motions involved in protein–ligand binary complex formation.

Materials and methods

Crystallization and X-ray data collection

MtCDA was concentrated to 12 mg/mL in sample buffer (20 mM Tris–HCl pH 7.5). Crystals of MtCDA were obtained using the vapor-diffusion hanging-drop method at 298.15 K using 24-well tissue-culture plates. Hanging drops were prepared by mixing 2 μL protein solution and 2 μL reservoir solution and placed over 400 μL reservoir solution containing 0.1 M Hepes pH 7.5 and 4.3 M sodium chloride. The ligands uridine (URD) and deoxyuridine (dURD) were added by soaking method.

The crystals were flash frozen at 100 K and cryoprotected with 20% of glycerol. X-ray diffraction data were collected at wavelength 1.431 Å using Synchrotron Radiation Source (Laboratório Nacional de Luz Síncrotron, Campinas, SP, Brazil) and CCD detector (MARCCD) with an exposure time of 1.6 s per image at a crystal to detector distance of 140 mm. X-ray diffraction data were processed using MOSFLM and scaled using SCALA [10].

Structure resolution and refinement

The crystal structures of MtCDA:URD and MtCDA:dURD were solved by molecular replacement with AMoRe package using the atomic coordinates of the structure 3IJF [8] as the search model. All waters molecules were removed from the search model and one monomer was employed in the molecular replacement. For structural refinement, the models were refined using *REFMAC5* [10] to give the final R_{factor} = 0.223 and R_{free} = 0.2905 to MtCDA: URD and R_{factor} = 0.227 and R_{free} = 0.257 to MtCDA:dURD. The *MOLPROBITY* web server [11] was used to generate the Ramachandran plots, and the percentage of residues in favored, allowed, and disallowed for MtCDA:URD are, 90.2%, 97.5%, and 2.5%, and for MtCDA:dURD are 96.7%, 97.5%, and 2.5%, respectively. All main chain angles, for all structures, are found in the most favorable or generally allowed regions.

Molecular dynamics simulation setup

All molecular dynamics (MD) simulations were carried out using the GROMACS 4.0.5 package [12] with the 53a6 GROMOS force field. We performed MD simulations for the enzyme in free form (PDB access code: 3IJF), and with the products (URD and dURD – PDB access code: 3LQP and 3LQT, respectively), in order to investigate the plasticity of the active site, and the interactions between the protein–ligand complex, and water molecules during the MD simulation.

The MD simulations were carried out using particle mesh Ewald method [13] for the electrostatic interactions. The van der Walls and Coulomb cutoff were 14 Å, and 10 Å, respectively. The integration time step was 2.0 fs, with the neighbor list being updated every 10 steps by using the grid option and a cutoff distance of 12 Å. The simple point charge extended (SPC/E) [14] water model was used. Periodic boundary condition has been used with constant number of particles, pressure, and temperature (NPT) in the system. The V-rescale thermostat was applied using a coupling time of 0.1 ps to maintain the systems at a constant temperature of 298.15 K. The Berendsen barostat was used to maintain the systems at pressure of 1 bar, and values of the isothermal compressibility set to 4.5×10^{-5} bar^{-1} for water simulations. The temperature of the systems were increased from 50 to 300 K in five steps (50–100 K, 100–150 K, 150–200 K, 200–250 K, and 250–300 K), and the velocities at each step were reassigned according to the Maxwell–Boltzmann distribution at that temperature and equilibrated for 10 ps, except the last part of thermalization phase, which was of 40 ps. The systems were subjected to a steepest descent followed by conjugated gradient energy minimizations until a tolerance of 1000 kJ/mol. MD simulation with position restraints was carried for a period of 20 ps in order to allow the accommodation of the water molecules in the system. Finally, 10 ns MD simulations were performed to all systems. The topologies files and other force field parameters except the charges of ligands were generated using the PRODRG program [15]. The partial atomic charges to the ligands were calculated using the Gaussian 03W package [16], which were submitted to single-point *ab initio* calculations at DFT/B3LYP/6-311G (2d, p) level in order to obtain ESP charges. In order to clarify the importance of the tetrameric structure of the MtCDA, MD simulations were carried out with the monomeric state, using the same protocol previously described.

Principal component analysis (PCA)

Essential dynamics (ED), also known as principal component analysis (PCA), is a method for identification of the main conformational changes, which often have importance in biological process, for a protein during an MD simulation.

In the ED analysis, a variance/covariance matrix was constructed from the trajectories after removal of the rotational and translational movements. Diagonalizing the matrix identified a set of eigenvectors and eigenvalues. The eigenvalues represented the amplitude of the eigenvectors along the multidimensional space, and the displacements of atoms along each eigenvector showed the concerted motions of protein along each direction. An assumption of ED analysis is that the correlated motions for the function of the protein are described by eigenvectors with large eigenvalues. The movements of protein in the essential subspace were identified by projecting the Cartesian trajectory coordinates along the most important eigenvectors from the analysis [17].

Results and discussion

Quaternary structure description

The final models (URD, dURD) were refined to, respectively, 2.4 and 1.9 Å resolution. The active site electron densities for complexes MtCDA:URD and MtCDA:dURD are presented in Fig. 2. Data collection and refinement statistics for all structures are given in

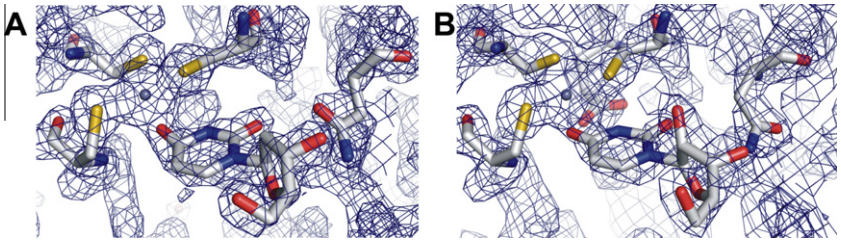

Fig. 2. Active site electron densities ($2F_{obs} - F_{calc}$) map for complexes MtCDA:dURD (A) and MtCDA:URD (B). The URD, dURD, and the residues are presented as sticks.

Table 1
Data collection and refinement statistics. Values in parentheses refer to the highest resolution shell.

Data collection and refinement statistics*	MtCDA:UDR	MtCDA:dURD
X-ray wavelenght (Å)	1.427	1.427
Temperature (K)	100	100
Resolution range (Å)	39.16 (2.40)	37.216 (1.90)
Space group	C222	C222
Matthews coefficient (Å^3 Da^{-1})	2.60	2.63
Unit-cell parameters		
a (Å)	65.92	65.41
b (Å)	78.33	77.59
c (Å)	56.73	55.68
$\alpha = \beta = \gamma$ (°)	90.00	90.00
Highest resolution shell (Å)	2.40	1.90
Data completeness (%)	99.90	92.9
R_{merge} (%)[a]	7.3	7.7
Resolution range used in refinement (Å)	28.41–2.40	28.20–1.90
R_{factor} (%)[b]	22.33	22.70
R_{free} (%)[c]	29.05	25.70
Observed RMSD from the ideal geometry		
Bond lenghts (Å)	0.041	0.023
Bond angles (°)	3.548	2.435
B values (Å)^2 [d]	24.065	25.524
Residues in most favored regions of the Ramachandran plot (%)	90.2	97
Residues in addicionally allowed regions of the Ramachandran plot (%)	7.3	2
Residues in generously allowed regions of the Ramachandran plot (%)	2.5	1
Residues in disallowed regions of the Ramachandran plot (%)	0	0
Number of ligands	1	1
Number of water molecules	93	50

[a] $R_{merge} = \sum_h \sum_i |I(h)_i - \langle I(h)\rangle| / \sum_h \sum_i I(h)_i$, where $I(h)$ is the intensity of reflection h, $\sum_h$ is the sum over all reflections and $\sum_i$ is the sum over i measurements.
[b] $R_{factor} = 100 \times \sum |F_{obs} - F_{calc}| / \sum (F_{obs})$, the sums being taken over all reflections with $F/\sigma(F) > 2$ cutoff.
[c] $R_{free} = R_{factor}$ for 10% of the data, which were not included during crystallographic refinement.
[d] *B* values = average *B* values for all non-hydrogen atoms.
* Values in parenthesis refer to the highest resolution shell.

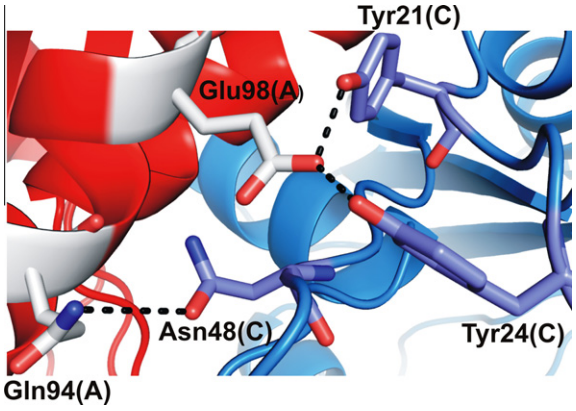

Fig. 3. Interface of the subunits A and C, showing the interactions between Glu98(A) with Tyr21(C), Tyr24(C), and Gln94(A) with Asn48(C). The protein is presented as cartoon and the residues as sticks.

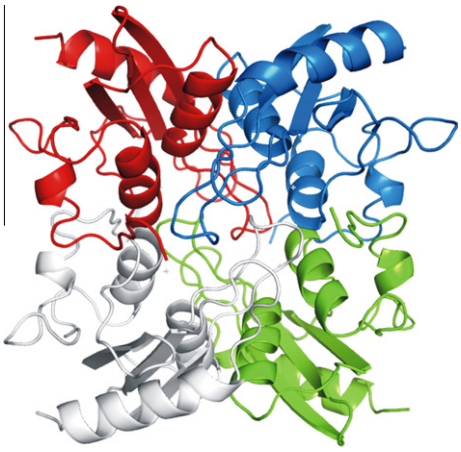

Fig. 4. Schematic drawing of tetrameric MtCDA. The protein is presented as cartoon and each monomer (A-red, B-blue, C-light grey, and D-green) is presented in different colors. This figure was generated using Chimera program [25]. (For interpretation of the references to colour in this figure legend, the reader is referred to the web version of this article.)

Table 1. The MtCDA monomer in complex with the products, follow the same arrangement α–β–α with a mixed β-sheet of five strands. These structures were crystallized in the space group C222. Examining the differences between MtCDA in free form and MtCDA complexed with products was observed that there are no major differences. The only changes are restricted to amino-acid side chains, which compose the active site. The RMSD value between apo structure and URD complex is 0.4 Å, and between apo structure and dUDR complex is 0.2 Å. Analysis of the interfaces reveals intermolecular contacts involving residues Tyr21–Glu98, Tyr24–Glu98, and Gln94–Asn48 of the adjacent subunits (A–C and B–D) (Fig. 3). In addition, analysis based on the web server PDBe PISA (Protein Interfaces, Surfaces and Assemblies) [18], reveals 23 hydrophobic interactions, and eight intermolecular hydrogen bonds between the adjacent subunits, and brought to light what seems to be a stable MtCDA quaternary structure (Fig. 4). Analyzing the contact areas between subunits of MtCDA:URD and MtCDA:dURD complexes, we suggest that the monomers can interact in three different ways. These different forms can be exemplified by the monomers A:B, A:C, and B:C, which are presented in the Fig. 5. Examining the interactions between A:B it was observed six hydrogen bonds and 17 hydrophobic contacts involving 23 residues, and the total area was 757.1 A^2. The total area for A:C was 1128.4 A^2, in addition 14 hydrogen bonds and

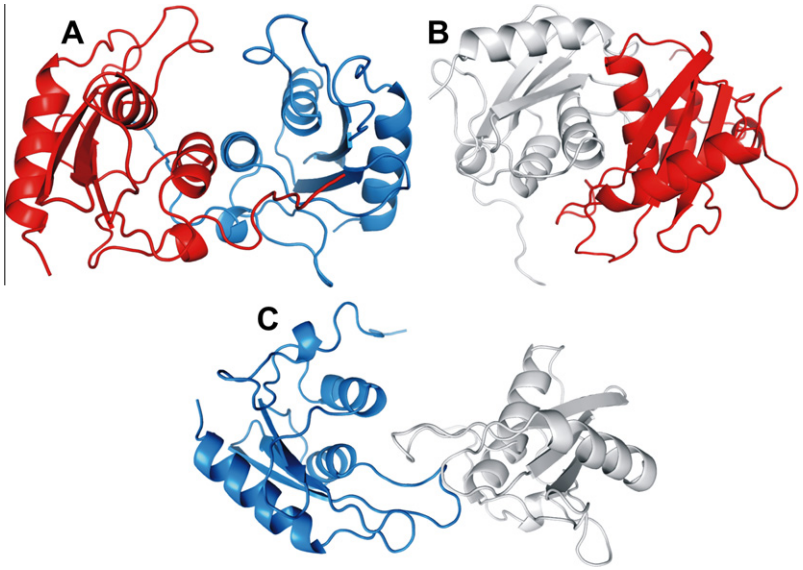

Fig. 5. The three interfaces contacts area, which are found to MtCDA:URD and MtCDA:dURD complexes. (A) Present A (red):B (blue); (B) A:C (light grey); and (C) B–C interfaces. (For interpretation of the references to colour in this figure legend, the reader is referred to the web version of this article.)

17 hydrophobic contacts involving 31 residues were observed. Finally, the region between B:C presents a total area of 412.1 A^2, which is composed by two hydrogen bonds and 10 hydrophobic contacts. Furthermore, in order to verify if these conformations are in agreement with CDA of different organism previously published, we analyzed other 13 CDA structures (PDB access codes: 3IJF, 3MPZ, 1MQ0, 3DMO, 1UX1, 2D30, 1UX0, 1UWZ, 1JTK, 2FR5, 1ZAB, 2FR6, and 3B8F) [19,20], which revealed the same packing presented by MtCDA.

Characterization of the product-binding pocket

The hydrogen bonding networks in the active site were determined from interactions between MtCDA and URD (MtCDA:URD) and dURD (MtCDA:dURD) products. Analysis of hydrogen bonds between URD and MtCDA reveals seven hydrogen bonds: six hydrogen bonds between the pyrimidine moiety and Cys89 (2.9 and 3.1 Å), Glu58 (3.4 and 3.2 Å), Cys92 (3.2 Å) and Ala57 (3.3 Å) residues, and one between the ribose moiety and Asn45 (3.2 Å) residue (Fig. 6). Additionally the complexes show two non-ligand residues, Phe27 and Cys56 which could be important in stabilizing hydrophobic interactions between the ligand and the enzyme and thereby facilitate the catalytic process, as reported for human CDA [21]. All of these interactions are located in the subunit A.

In contrast, some differences were found in the active site between MtCDA:dURD binary complex and apo MtCDA, which involve subunits A and D. This complex reveals seven hydrogen bonds, three with pyrimidine Cys89 (2.9 Å), Glu58 (2.9 Å), Ala57 (3.3 Å) and four with ribose involving residue Asn45 (2.7 Å), Glu47 (2.8 Å), Tyr51(D) (3.1 Å), and Val49(D) (2.9 Å).

Three cysteine residues (Cys56, Cys89, and Cys92) are involved in zinc metal binding. However, only Cys56 is involved in hydrophobic contacts, as previously mentioned. The properties of the Cys56 (Cys65 human CDA numbering) suggested it is required for the enzymatic activity but not for the maintenance of zinc in the active site, whereas Cys65 (human CDA) plays a role in placing the zinc ion in the correct position and orientation within the active site [22]. Table S1 summarizes the interaction between *Mt*CDA:URD and dURD. Analyzing the three main regions, which are described to all tetrameric CDAs, we observed some differences that could be a guide to future rational drug design studies aiming

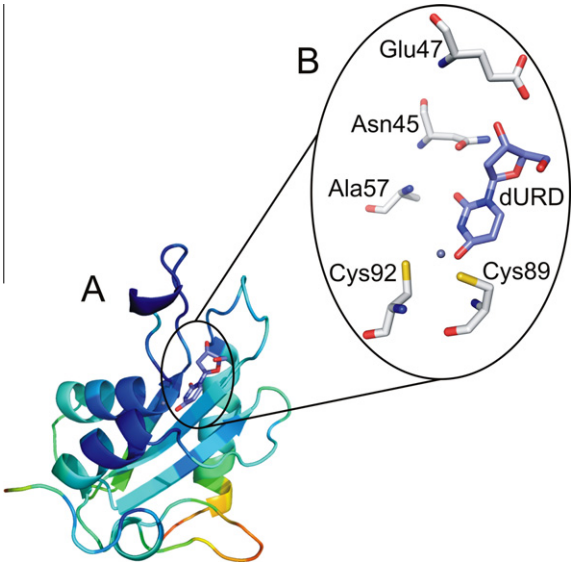

Fig. 6. Classical binding site of the MtCDA:dURD anchored by the residues Asn45, Glu47, Ala57, Cys89, and Cys92, which are important residues of the binding pocket. The protein is presented as cartoon and the binding site residues as sticks.

to find selective inhibitors to *Mt*CDA. In the first region, close to the active site, which comprises $_{32}$PYS**H**F$_{36}$ (human CDA) and $_{23}$PYS**R**F$_{27}$ (*Mt*CDA), the replacement of a histidine by an arginine does not implies physical chemistry changes. However, considering torsion angles, arginine presents increased entropy, which could influence ligand recognition. It is should be pointed that Tyr33, already characterized as a pivotal residue involved in the quaternary structure organization in human CDA [23], is conserved in both sequences, and could be playing the same role in *Mt*CDA. The second region comprises the residues $_{57}$N**AC**Y**P**$_{61}$ (human CDA) and $_{48}$N**VS**Y**G**$_{52}$ (*Mt*CDA). Three replacements are observed in this sequence. The first, an alanine residue was changed by a valine did not implied major structural difference, although valine presents one more torsion angle when compared to alanine. The replacement of a cysteine by a serine, involves of a thiol (Cys) and hydroxyl groups (Ser). However, both residues can participate

in hydrogen bonding. The last change in this sequence is the presence of a proline in human CDA and a glycine in *Mt*CDA. Finally, the last analyzed region, conserved in all T-CDAs, comprises the residues $_{65}$CAE**RTA**$_{70}$ in human CDA and $_{56}$CAE**CAV**$_{61}$ in *Mt*CDA. We observed that Arg68, described as an important residue in the catalytic event in the human CDA [24], compensating the negative charges of the cysteines, corresponds to a cysteine in *Mt*CDA. Nevertheless, analyzing the *Mt*CDA structure, it could be suggested that the residue responsible for counterbalancing the charges of the cysteines is Arg91, which is not conserved in the human CDA, where it corresponds to Ala101. Taking these differences in consideration, MtCDA presents peculiarities close to the active site, when compared to human CDA, which could be involved in the ligand recognition process and can provide some clues to rational drug design initiatives.

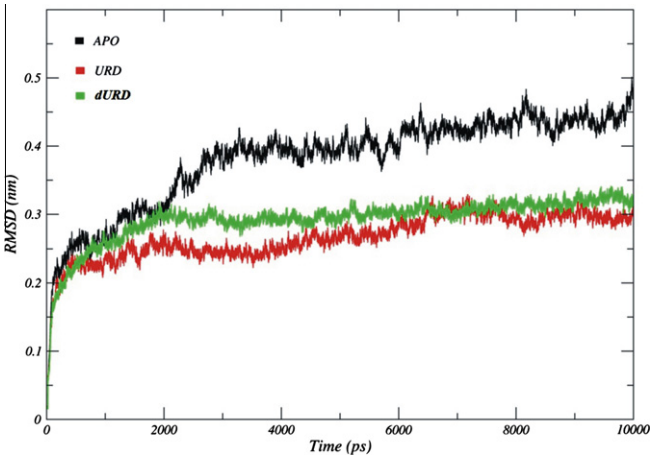

Fig. 7. Graphical representation of RMSD of each MtCDA structure from starting structure of tetramers as a function of time, over 10 ns of simulation.

Dynamics simulation and essential dynamics

In order to understand the stability of the MtCDA in solution during the simulation, the C–α root means square deviation (RMSD) was calculated (Fig. 7). The MtCDA in the apo form and in complex with either URD or dURD achieved a plateau within 2500 and 2000 ps, respectively, suggesting that ~10 ns is sufficient for stabilizing fully relaxed models. As shown in Fig. 7, the RMSD values in the MtCDA:URD and dURD remain less 3.0 Å, whereas in the apo form was less than 5.0 Å. These results suggest that the MtCDA when in complex with products presents a more stable system than the structure in absence of these ligands in the binding pocket. To analyze the physically relevant motions of the simulations, the principal components (PC) were calculated by diagonalizing the covariance matrix generated from timescale

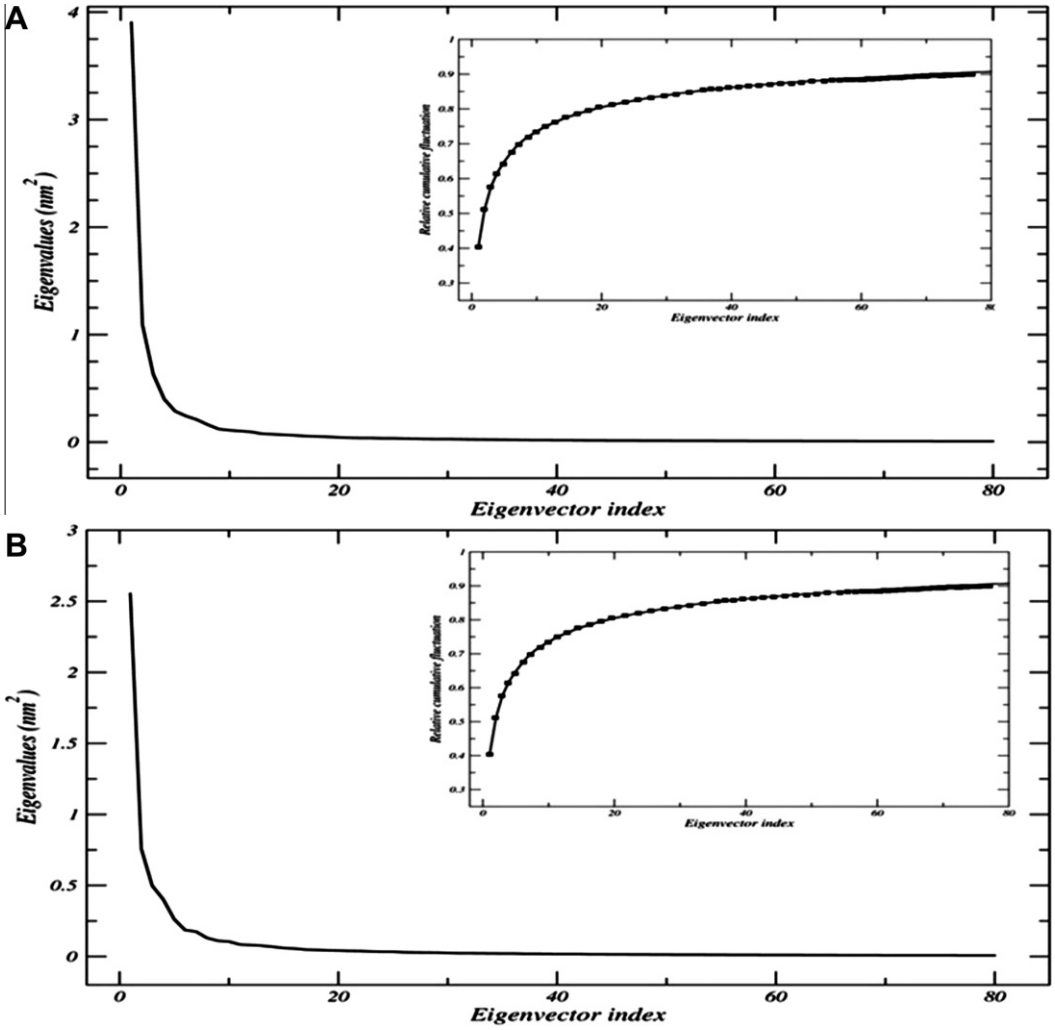

Fig. 8. Eigenvalues of the covariance matrix resulting from the simulations of the MtCDA:dURD (A) and MtCDA:URD (B) complexes.

(10 ns) explicit solvent MD simulation. The anharmonic and large-scale motions of the protein are isolated from the mostly harmonic and small-scale motion. Knowing that the large-scale anharmonic motions in the essential subspace are often correlated to the pivotal functions of the protein, we have only focused on these movements. The analysis of the first 50 eigenvectors describes 87.71% (dURD) and 85.33% (URD) of the fluctuations during the simulation, and the first eigenvector of each simulation correspond of ~40% of the total of 1488 eigenvectors (Fig. 8).

Flexibility of the product-binding pocket

In this section, we analyzed the main fluctuations of the MtCDA in complex with its products in comparison with the structure in apo form. Fig. 9 presents the most relevant fluctuations, obtained from the first eigenvector, of the monomer A during the simulation. Based on these results, it could be highlighted three principal regions that will be denominated R1, R2, and R3. The R1 region, that comprises residues Val22–Phe27, is located in the monomer interface, being crucial for the stabilization of the quaternary structure. Furthermore, it was observed the approximation of Tyr24 to Glu98 of the adjacent subunit, corroborating with the analysis previously published [9]. As an understanding of product binding to, and release from, the enzyme active site is pivotal to elucidate the MtCDA mode of action, the R2 region was analyzed. R2 comprises residues Thr42–Cys56. Analyzing the active site of the monomer A, one can observe three main interactions, made by Asn45, Glu47, and Cys56 contributing for the stability of the ligands into the binding cavity. In addition, it was also observed that Val49 and Tyr51 belong to the binding site of the monomer D. The R3 region is composed by Val110–Phe123 and is located close to the adjacent binding site (A–B and C–D). In this region we also detect π–π stacking interactions involving the pyrimidine moiety of the products and Phe123, contributing to ligand binding.

Tetramer vs monomer: the ligand stability based on dihedral analysis

In order to access the importance of the quaternary structure to the ligand stability into the binding pocket, we carried out MD simulations with the MtCDA in monomeric form. To analyze the stability of ligand in these two scenarios (tetramer and monomer) we monitored dihedral angle of the products (C6:N1:C1∗:O4∗) and the electrostatic interaction (*Coulomb – Short Range*) between protein–ligand complexes for the period of the simulation. Fig. S1 presents the dihedral angle that was evaluated, and Figs. S2 (URD) and S3 (dURD) show the dihedral angle and energy interaction during the simulations. The total number of transitions, considering the dihedral angle, was 97 for the monomeric structure (URD and dURD), 11 for tetramer complexed with URD and 39 when associated with dURD. In addition, the transitions of the dihedral angle in the tetramer have a direct influence in the electrostatic interactions, suggesting that, for a proper stabilization of the ligand into the binding site, the quaternary structure is required. When the average of the electrostatic interactions in the tetrameric and monomeric structures in complex with the products were compared, it was clear that the structure that enabled the most stable form of the ligand was the tetramer. Table S2 summarizes these findings.

The dynamics motions of the ligands (URD and dURD) were analyzed via characterization of the phase space behavior. Fig. 10 present the trajectory of the first two principal components (PC1 and PC2), taking into account the motions of the ligands in the phase space. As shown in Fig. 10A and B, we can identify three clusters of stable states for the ligands when in complex with monomeric structures. In contrast, Fig. 10C and D present only one cluster, defining only one stable state for the ligands. These results could be related with the stability of the ligand in the binding site, and justify the use of the quaternary structure for future studies of potential inhibitors to MtCDA. Furthermore, as described above, these results corroborate the importance of the adjacent subunits

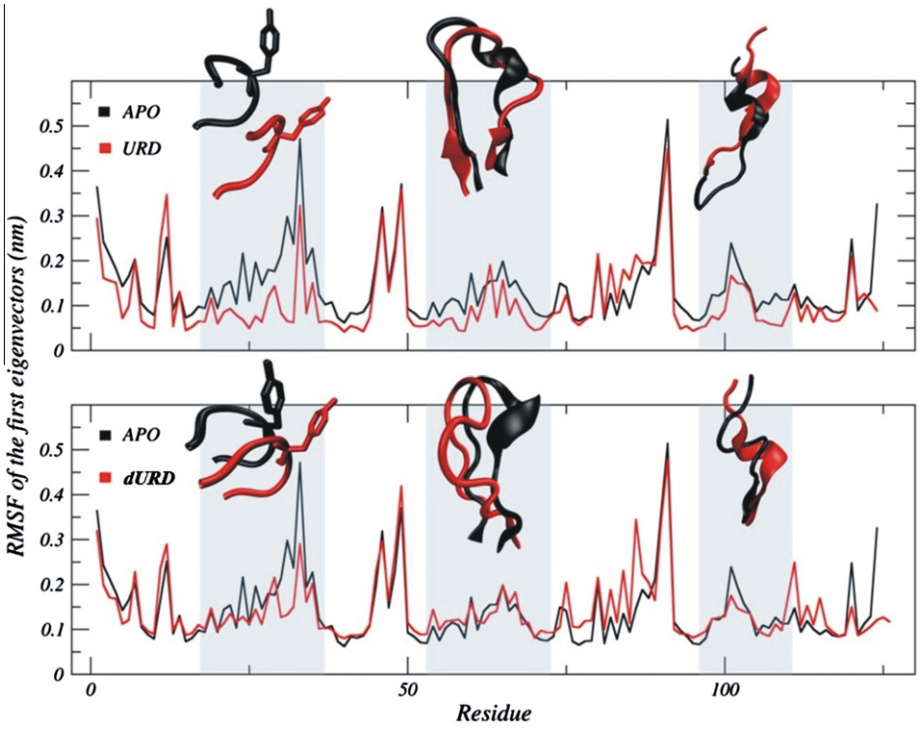

Fig. 9. Displacement of the components of the first eigenvectors for tetrameric structures of unbound MtCDA, MtCDA:URD and MtCDA:dURD complexes. The main fluctuations are presented for the regions R1 (Val22–Phe27), R2 (Thr42–Cys56) and R3 (Val110–Phe123). The main residues, which composed the regions described above, are presented as cartoon in order to facilitate the interpretation.

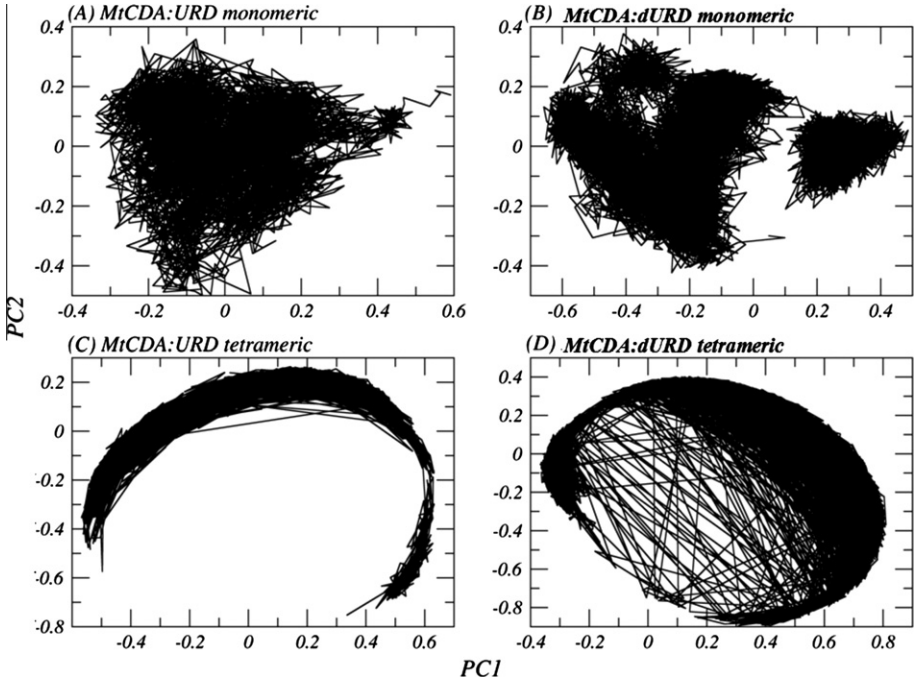

Fig. 10. Dynamics motions of the ligands (URD and dURD) were analyzed via characterization of the phase space behavior when in complex with either a tetrameric or a monomeric structure. (A and B) Trajectory of the first two principal components to URD and dURD, respectively, when associated with MtCDA monomeric form; (C and D) trajectory of the first two principal components to URD and dURD, respectively, when associated with MtCDA tetrameric form.

residues Val49 (monomer D), Tyr51 (monomer D), and Phe123 (monomer B) for stability of the ligand into the binding pocket, since in absence of these residues, the MtCDA reaction product does not remain in the active site during MD simulations.

Conclusions

The present study provided, for the first time, structural insight into the product binding patterns for MtCDA, elucidating the main residues involved in proper binding of products. In addition, our results highlight that the MtCDA quaternary structure follows the same packaging, which is observed in others CDAs from different organisms. Analysis of the active site revealed that the Asn45, Glu47, Ala57, Cys89, and Cys92 amino acid residues are pivotal to product recognition by MtCDA. The MD simulations corroborated with the proposed packing, showing that residues Tyr51, Val49, and Phe123 present an important role in the active site of the adjacent subunits (A–D and B–C). Simulations of the tetrameric and monomeric MtCDA structures suggest that the oligomeric state is essential for stabilization of the ligand into the enzyme-binding site, lending support to the importance of protein–protein interactions. In summary, these findings open-up the possibility to use MtCDA as a target in future studies aiming to the rational design of new inhibitor of MtCDA-catalyzed chemical reaction with potential anti-proliferative activity on cell growth of *M. tuberculosis*, the major causative agent of tuberculosis.

Deposit

The atomic coordinates have been deposited in the PDB (complexes MtCDA:URD and MtCDA:dURD – PDB access codes: 3LQP and 3LQT, respectively).

Acknowledgments

This work was supported by National Institute of Science and Technology on Tuberculosis (Decit/SCTIE/MS-MCT-CNPq-FNDCT-CAPES). D.S.S. (304051/1975-06), L.A.B. (520182/99-5), and W.F.A. Jr. (300851/98-7) are research career awardees of the National Council for Scientific and Technological Development of Brazil (CNPq). R.A.C. acknowledge a scholarship awarded by CNPq. L.F.S.M.T. and Z.A.S.Q. acknowledges a scholarship awarded by CAPES.

Appendix A. Supplementary data

Supplementary data associated with this article can be found, in the online version, at doi:10.1016/j.abb.2011.01.022.

References

[1] R. Cohen, R. Wolfenden, J. Biol. Chem. 246 (1971) 7561–7565.
[2] D.F. Wentworth, R. Wolfenden, Metthods Enzymol. 51 (1978) 401–407.
[3] A. Somasekaram, A. Jarmuz, A. How, J. Scott, J. Biol. Chem. 274 (1999) 28405–28412.
[4] S.J. Chung, C. Fomme, G. Verdine, J. Med. Chem. 48 (2005) 658–660.
[5] E. Johansson, N. Mejlhede, S. Larsen, Biochemistry 41 (2002) 2563–2570.
[6] P. Itapa, G. Cercignani, E. Balestreri, Biochemistry 9 (1970) 3390–3395.
[7] L. Betts, S. Xiang, S.A. Short, R. Wolfenden, C.W. Carter, J. Mol. Biol. 235 (1994) 635–656.
[8] Z.A. Sánchez-Quitian, C.Z. Schneider, R.G. Ducati, W.F. de Azevdo Jr., C. Bloch, L.A. Basso, D.S. Santos, J. Struct. Biol. 169 (2010) 413–423.
[9] D. Carlow, C. Carter, N. Mejhede, R. Wolfenden, Biochemistry 38 (1999) 12258–12265.
[10] CCP4, Collaborative Computational Project Number 4, Acta Cryst. D. 50 (1994) 760–763.
[11] I.W. Davis, L.W. Murray, J.S. Richardson, D.C. Richardson, Nucleic Acids Res. 32 (2004) W615–W619.
[12] D. van der Spoel, E. Lindahl, B. Hess, G. Groenhof, A.E. Mark, H.J.C. Berendsen, J. Comput. Chem. 26 (2005) 1701–1718.
[13] T. Darden, D. York, L. Pedersen, J. Chem. Phys. 98 (1993) 10089–10092.
[14] H.J.C. Berendsen, J.P.M. Postma, W.F. van Gunsteren, J. Hermans, Interaction models for water in relation to protein hydration, in: B. Pullman (Ed.), Intermolecular Forces, D. Reidel Publishing Company, Netherlands, 1981.
[15] D.M.F. van Aalten, B. Bywater, J.B.C. Findlay, M. Hendlich, R.W.W. Hooft, G.J. Vriend, J. Comput. Aided Mol. Des. 10 (1996) 255–262.
[16] M.J. Frisch, G.W. Trucks, H.B. Schlegel, G.E. Scuseria, M.A. Robb, J.R. Cheeseman, V.J. Zakrzewski, J.A. Montgomery, R.E. Stratmann, J.C. Burant, S. Dapprich, J.M. Millam, A.D. Daniels, K.N. Kudin, M.C. Strain, O. Farkas, J. Tomasi, V. Barone, M. Cossi, R. Cammi, B. Mennucci, C. Pomelli, C. Adamo, S. Clifford, J. Ochterski, G.A. Petersson, P.Y. Ayala, Q. Cui, K. Morokuma, D.K. Malick, A.D. Rabuck, K.

Raghavachari, J.B. Foresman, J. Cioslowski, J.B. Ortiz, B.B. Stefanov, G. Liu, A. Liashenko, P. Piskorz, I. Komaromi, R. Gomperts, R.L. Martin, D.J. Fox, T. Keith, M.A. Al-Laham, C.Y. Peng, A. Nanayakkara, C. Gonzalez, M. Challacombe, P.M.W. Gill, B.G. Johnson, W. Chen, M.W. Wong, J.L. Andres, M. Head-Gordon, E.S. Replogle, J.A. Pople, Gaussian 03, Gaussian, Wallingford, CT, 2003.
[17] A. Amadei, A.B.M. Linssen, H.J.C. Berendsen, Proteins 17 (1993) 412–425.
[18] E. Krissinel, K. Henrick, J. Mol. Biol. 372 (2007) 774–797.
[19] E. Johansson, J. Neuhard, M. Willemoes, S. Larsen, Biochemistry 43 (2004) 6020–6029.
[20] A.-H. The, M. Kimura, M. Yamamoto, N. Tanaka, I. Yamaguchi, T. Kumasaka, Biochemistry 45 (2006) 7825–7833.
[21] S. Vincenzetti, G. De Sanctis, S. Costanzi, G. Cristalli, P. Mariani, G. Mei, J. Neuhard, P. Natalini, V. Polzonetti, A. Vita, Protein Eng. 16 (2003) 1055–1061.
[22] A. Cambi, S. Vincenzetti, J. Neuhard1, S. Costanzi, P. Natalini, A. Vita, Protein Eng. 11 (1998) 59–63.
[23] D. Micozzi, S. Pucciarelli, F.M. Carpi, S. Costanzi, G. De Sanctis, V. Polzonetti, P. Natalini, I.F. Santarelli, A. Vita, S. Vincenzetti, Int. J. Biol. Macromol. 47 (2010) 471–482.
[24] S. Vincenzetti, B. Quadrini, P. Mariani, G. De Sanctis, N. Cammertoni, V. Polzonetti, S. Pucciarelli, P. Natalini, A. Vita, Proteins 70 (2008) 144–156.
[25] E.F. Pettersen, T.D. Goddard, C.C. Huang, G.S. Couch, D.M. Greenblatt, E.C. Meng, T.E. Ferrin, J. Comput. Chem. 25 (2004) 1605–1612.